



CHORUS

This is the accepted manuscript made available via CHORUS. The article has been published as:

Virtual Trions in the Photoluminescence of Monolayer Transition-Metal Dichalcogenides

Dinh Van Tuan, Aaron M. Jones, Min Yang, Xiaodong Xu, and Hanan Dery

Phys. Rev. Lett. **122**, 217401 — Published 29 May 2019

DOI: [10.1103/PhysRevLett.122.217401](https://doi.org/10.1103/PhysRevLett.122.217401)

Virtual trions in the photoluminescence of monolayer transition-metal dichalcogenides

Dinh Van Tuan,¹ Aaron M. Jones,² Min Yang,¹ Xiaodong Xu,^{2,3} and Hanan Dery^{1,4,*}

¹*Department of Electrical and Computer Engineering,
University of Rochester, Rochester, New York 14627, USA*

²*Department of Physics, University of Washington, Seattle, Washington 98195, USA*

³*Department of Materials Science and Engineering,
University of Washington, Seattle, Washington 98195, USA*

⁴*Department of Physics and Astronomy, University of Rochester, Rochester, New York 14627, USA*

Photoluminescence experiments from monolayer transition-metal dichalcogenides often show that the binding energy of trions is conspicuously similar to the energy of optical phonons. This enigmatic coincidence calls into question whether phonons are involved in the radiative recombination process. We address this problem, unraveling an intriguing optical transition mechanism. Its initial state is a localized charge (electron or hole) and delocalized exciton. The final state is the localized charge, phonon and photon. In between, the intermediate state of the system is a virtual trion formed when the localized charge captures the exciton through emission of the phonon. We analyze the difference between radiative recombinations that involve real and virtual trions (i.e., with and without a phonon), providing useful ways to distinguish between the two in experiment.

PACS numbers:

The coupling between phonons and charged particles in monolayer transition-metal dichalcogenides (ML-TMDs) exhibits unique behavior due to their atomically thin nature. In addition to a strong Fröhlich interaction [1–4], thickness fluctuations of the ML due to homopolar optical phonons decrease charge mobility [5], while soft undulations of the ML due to acoustic flexural phonons enhance spin relaxation [6, 7]. In the context of optical properties, phonons induce decoherence, energy relaxation, and mass change of exciton complexes [7–19]. A noticeable property is that the Raman-active phonon energies nearly resonate with the energy difference between the exciton and trion spectral lines (binding energy of the trion) [20, 21]. This energy proximity has often led to widespread confusion in the assignment of optical transitions in photoluminescence (PL) experiments.

We explain the confusion by inspecting the experimental data in Fig. 1. The top panels show the normalized PL from MoSe₂, WSe₂, WS₂, and MoS₂ (left to right), where all the MLs are unintentionally *n*-type and all are supported on Si/SiO₂ substrates. For details on the experiment, see Ref. [22]. In each case, the emission spectra have two peaks where the higher energy one is attributed to neutral excitons (X^0). Typically, it is tempting to attribute the low-energy peak to negative trions because some of these peaks also appear in the absorption spectra when electrons are added to the ML through a gate voltage [23–25]. However, when performing Raman spectroscopy on the same samples (lower panels of Fig. 1), we find that the energy of the dominant Raman-active phonon mode matches the energy difference between X^0 and the low-energy peak in the PL. This systematic behavior raises the question: Does the low energy peak in the PL stem from recombination of real trions or is it

phonon-assisted recombination of excitons? This important question is addressed in this Letter.

Phonon-assisted optical transitions of neutral excitons, governed by the Fröhlich interaction [26–29], are weak in ML-TMDs. It is a result of the charge neutrality and small size of the exciton as well as the similar effective masses of electrons and holes. Combined together, the interactions of the electron and hole with the phonon-induced macroscopic electric field cancel out [18]. We offer an alternative phonon-assisted recombination scenario facilitated by virtual trion states. Here, the strong Fröhlich coupling between a localized electron (or hole) and the lattice is used to capture a nearby exciton by emission of a phonon. The capture mechanism is considered virtual during radiative recombination if $\Delta E = E_T + E_\lambda - E_X - E_\ell \neq 0$, where the energies are of the localized trion (E_T), exciton (E_X), localized charge (E_ℓ), and phonon (E_λ). Energy conservation dictates that the exciton is converted to a phonon plus photon. Furthermore, if ΔE is close to zero, the emission spectrum includes a single dominant phonon-assisted optical transition instead of a series of phonon-replicas that decay according to the standard Huang-Rhys analysis [30].

We begin the analysis by solving the Schrödinger Equation of an \mathcal{N} -particle system with the Hamiltonian

$$H_{\mathcal{N}} = \sum_i^{\mathcal{N}} V_E(r_i, z) - \frac{\hbar^2}{2m_i} \nabla_i^2 + \sum_{i<j}^{\mathcal{N}} V_I(r_{ij}). \quad (1)$$

The particles are influenced by a point-charge defect in the substrate whose distance from the mid-plane of the ML is z , as shown by Fig. 2(b). $V_E(r_i, z)$ is the Coulomb interaction between this extrinsic defect and the i^{th} particle in the ML. The effective mass of the latter is m_i .

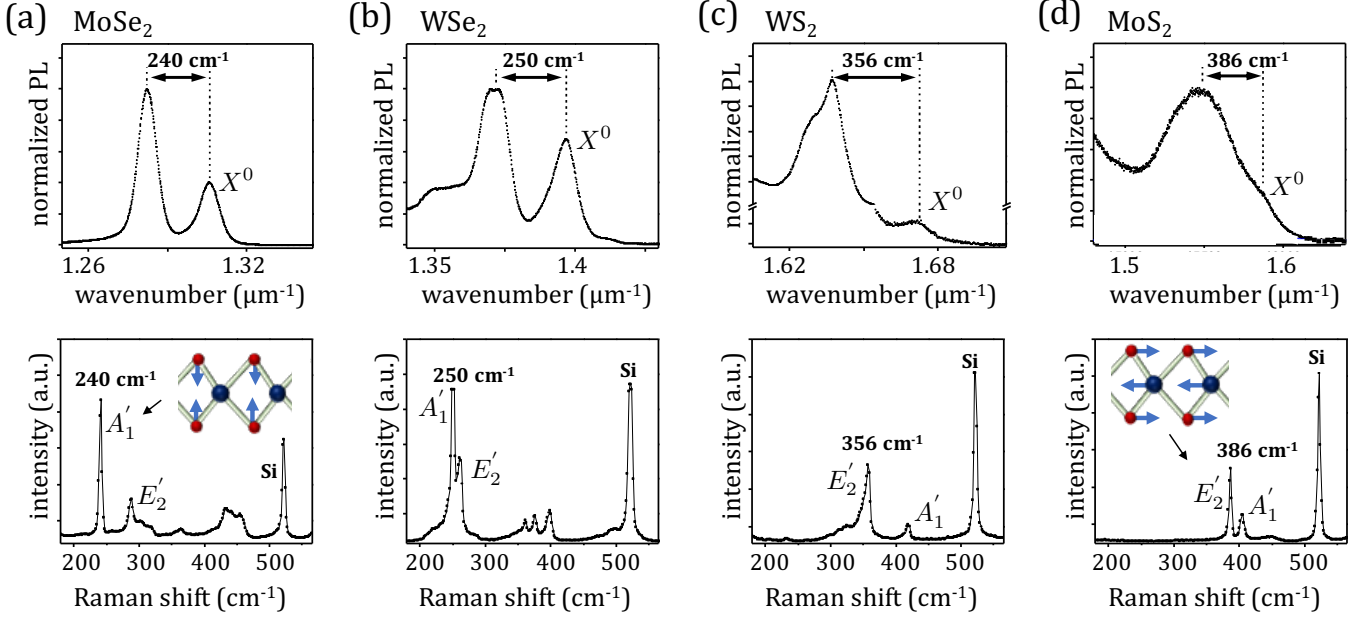


FIG. 1: (a)-(d) Normalized PL (top) and Raman spectra (bottom) of common ML-TMDs supported on Si/SiO₂ substrates. The normalized PL includes the neutral exciton peak (X^0) and a peak that is commonly associated with the negatively-charged trion in n -type samples. The energy difference between these peaks matches the energy of the dominant Raman active phonon mode in each of the MLs, as is readily seen in the top and bottom panels. The active Raman phonons are the homopolar and longitudinal-optical modes, denoted by A_1' and E_2' , respectively. Their atomic displacements are indicated in the insets of (a) and (d). The Raman spectra also show the active optical phonon mode of the Si substrate around 520 cm^{-1} .

$V_1(r_{ij})$ is the Coulomb interaction between the i^{th} and j^{th} particles where $r_{ij} = |\mathbf{r}_i - \mathbf{r}_j|$. It is relevant when $\mathcal{N} \geq 2$. The supplemental information includes details on the Coulomb interactions and parameter values we use in the simulations. Equation (1) is solved for localized electrons ($\mathcal{N}=1$), excitons ($\mathcal{N}=2$), and trions ($\mathcal{N}=3$) by the Stochastic Variational Method (SVM)[18, 31–35].

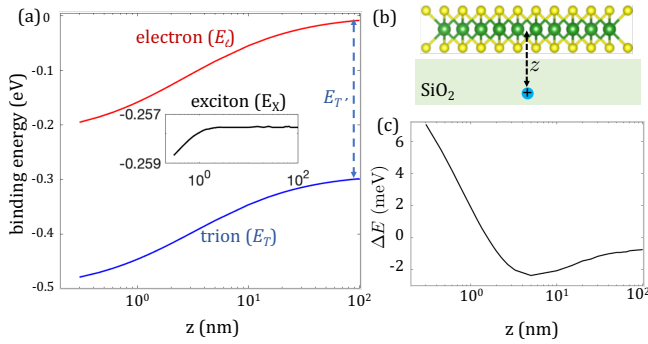


FIG. 2: (a) Ground-state energies of electrons (E_ℓ), excitons (E_X , inset), and negative trions (E_T) in ML-WSe₂ supported on SiO₂ substrate as a function of the distance of a positive point-charge defect from the mid-plane of the ML. $E_{T'}$ denotes the energy of delocalized trions ($z \rightarrow \infty$). (b) A cartoon of the ML, substrate and extrinsic defect. (c) $\Delta E = (E_T + E_\lambda) - (E_X + E_\ell)$, where $E_\lambda = 32 \text{ meV}$ is the phonon energy.

Figure 2(a) shows the calculated energies in ML-WSe₂ when a $+1e$ charged defect is embedded in SiO₂. The electron binding energy is largest when the defect is at the surface, $E_\ell(z = 0.3 \text{ nm}) \sim 200 \text{ meV}$. A similar localization-induced enhancement is seen in the energy of the trion (E_T). On the other hand, excitons are essentially unaffected by the defect, as shown by the inset. The weak dependence stems from the confluence of exciton neutrality and lack of contact between extrinsic defects and electrons or holes in the mid-plane of the ML. Similarly, $E_T - E_\ell$ is also largely independent of z because the defect interacts weakly with the added electron-hole pair in the trion complex. Figure 2(c) shows the value of $\Delta E = (E_T + E_\lambda) - (E_X + E_\ell)$, where $E_\lambda = 32 \text{ meV}$ is the energy of the phonon [24].

Next, we analyze interactions that facilitate the capture process. When the magnitude of their matrix elements is comparable or larger than $|\Delta E|$, the phonon-assisted optical transitions display a strong resonance in the emission spectra. The matrix element reads

$$M_\lambda(\mathbf{K}, \mathbf{q}) = \langle \Psi_T | \sum_j \beta_j D_{j,\lambda}(\mathbf{q}) e^{i\mathbf{q}\cdot\mathbf{r}_j} | \Psi_X(\mathbf{K}) \Psi_\ell \rangle, \quad (2)$$

where $\lambda = \{A_1', E_2'\}$ is the phonon mode (Fig. 1). \mathbf{q} and \mathbf{K} are the phonon and exciton wavevectors, respectively. The localized electron (trion) state is denoted by Ψ_ℓ (Ψ_T). The exciton in the initial state is delocalized, $\Psi_X(\mathbf{K}) = \varphi_X(r) e^{i\mathbf{K}\cdot\mathbf{R}} / \sqrt{A}$, where $r = |\mathbf{r}_e - \mathbf{r}_h|$ and $\mathbf{R} = (m_e \mathbf{r}_e + m_h \mathbf{r}_h) / (m_e + m_h)$ are the relative

and center-of-mass coordinates, respectively. A is the area of ML. The sum over j takes into account the long-range Fröhlich interaction between the j^{th} particle and longitudinal-optical phonons, $D_{j,E'_2}(\mathbf{q})$, or the short-range interaction of the particle with homopolar phonons, $D_{j,A'_1}(\mathbf{q})$. $\beta_j = 1$ ($\beta_j = -1$) when the j^{th} particle is an electron (hole). The supplemental information file includes technical details of these interactions, along with a compiled list of all the parameters we use.

The rate of the phonon-assisted recombination of neutral excitons mediated by localized electrons reads [36]

$$\frac{1}{\tau_\lambda(\mathbf{K})} = \left[\frac{1}{2}(1 \pm p_\ell)n_d A \cdot \frac{\sum_{\mathbf{q}} |M_\lambda(\mathbf{K}, \mathbf{q})|^2}{(\Delta E - E_K)^2 + \Gamma^2} \right] \frac{1}{\tau_\ell}, \quad (3)$$

where n_d is the density of localized electrons due to extrinsic defects, Γ is the broadening parameter, and $E_K = \hbar^2 K^2 / 2M$ is the exciton kinetic energy ($M = m_e + m_h$). τ_ℓ is the radiative decay time of a localized trion. The term $(1 \pm p_\ell)/2$ denotes the change in the recombination rate when the localized electron system becomes spin-polarized ($p_\ell \neq 0$) because of a strong magnetic field or magnetic proximity effects [37]. In more detail, a delocalized exciton can be captured only if the spin of its electron component is opposite to that of the localized electron (the valley degree of freedom is not a good quantum number for localized electrons, and therefore localized trions can only appear in a singlet-spin configuration [36]). When the localized electrons are spin-polarized, the phonon-assisted recombination rate is enhanced for one exciton branch, $(1 + p_\ell)/2$, while it is suppressed for the other, $(1 - p_\ell)/2$. Below, we focus on the non-magnetic case ($p_\ell = 0$). The supplemental material includes a discussion of the magnetic case along with interpretation of recent related experiments.

The expression inside square brackets in Eq. (3), hereafter denoted by $C_\lambda(\mathbf{K})$, is unit-less and it represents the amplitude of the virtual capture process. Figure 3(a) shows its value when $n_d = 4 \times 10^{11} \text{ cm}^{-2}$ for the Fröhlich interaction, $\lambda = E'_2$, in three different regimes with $\Delta E > 0$, $\Delta E \simeq 0$, and $\Delta E < 0$. As shown in Fig. 2(c), ΔE is positive for surface defects ($z \lesssim 1.5 \text{ nm}$). Following Eq. (3), the capture amplitude in this case is optimal when $E_K = \Delta E$. For farther impurities, on the other hand, the capture amplitude decreases monotonically because $\Delta E \leq 0$. The general trends in Fig. 3(a) are that faster excitons are less prone to the capture process, and that the capture is weaker when the defect is remote. The latter reassures the important role of localization. It is so because $M_\lambda(\mathbf{K}, \mathbf{q})$ is sizable when $q\ell_e \lesssim 1$, where ℓ_e is the characteristic electron localization length. That is, tighter localization enables more phonons to be involved in the capture process and contribute effectively to the sum in Eq. (3). In addition, the overlap between the initial and final states in Eq. (2) is optimal for nearby defects because ℓ_e becomes comparable to both the exci-

ton Bohr radius and the characteristic distances between the particles of the trion complex.

We compare the recombination rates of delocalized excitons with and without phonons. The effective rate of the phonon-assisted process mediated by localized electrons follows from the average

$$\left\langle \frac{1}{\tau_\lambda(\mathbf{K})} \right\rangle = \frac{\sum_{\mathbf{K}} f_X(\mathbf{K}) / \tau_\lambda(\mathbf{K})}{\sum_{\mathbf{K}} f_X(\mathbf{K})}, \quad (4)$$

where $f_X(\mathbf{k})$ is the distribution function of delocalized excitons. The effective rate of the direct recombination reads [38]

$$\frac{1}{\tau_0} = \left[\frac{(\hbar\omega_0)^2}{2k_B T M c^2} \right] \frac{1}{\tau_X}. \quad (5)$$

$\hbar\omega_0 = E_g - |E_X|$ is the resonance photon energy where E_g is the band-gap energy. c is the speed of light in vacuum and $k_B T$ is the thermal energy. τ_X is the radiative decay time of delocalized excitons in the light cone. It is typically the fastest decay process [39, 40]. The term in square brackets denotes the strong attenuation after averaging over the distribution of excitons. It is about 0.01 already at $T = 5 \text{ K}$, reflecting the fact that only a negligible fraction of delocalized excitons reside in the light cone (excitons whose kinetic energy is of the order of a few μeV). We do not consider the acoustic-phonon-assisted recombination of delocalized excitons in our analysis ('pushing' the excitons into the light cone by emission of low-energy phonons). The main effect of acoustic phonons is to broaden the high-energy tail of X^0 and not to strongly amplify the emission [19].

Figure 3(b) shows the calculated normalized PL for a Boltzmann distribution of excitons at $T = 5 \text{ K}$. We notice that while the amplitude of the capture process depends on how far the extrinsic defect is from the ML, as shown in Fig. 3(a), the energy of the emitted photon does not, as

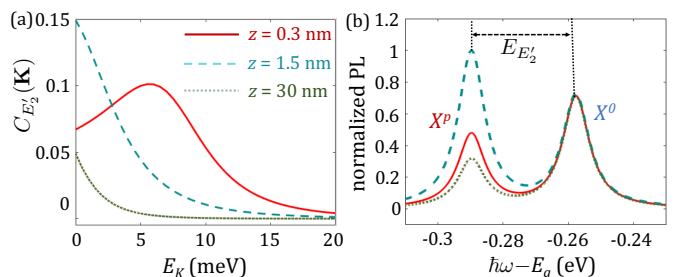


FIG. 3: (a) The capture parameter, $C_{E'_2}(\mathbf{K})$, as a function of the exciton kinetic energy when $n_d = 4 \times 10^{11} \text{ cm}^{-2}$. (b) The PL spectrum for the corresponding cases in panel (a) at $T = 5 \text{ K}$ and $\tau_\ell = 10\tau_X$. To account for disorder, an inhomogeneous broadening of $\Gamma = 5 \text{ meV}$ has been used. The simulations use the parameters of ML-WSe₂ supported on SiO₂ substrate.

shown in Fig. 3(b). Namely, the spectral line always appears at E_λ below X_0 . Consequently, the resonance photon energies are similar in devices in which the defects are concentrated at a certain distance from the ML, and others in which the defects are uniformly distributed in the substrate. Figure 3(b) shows that the emission from delocalized excitons in the light cone is comparable with the phonon-assisted recombination. The intensity ratio between the phonon-related peak (X^p) and the delocalized exciton peak (X^0) is commensurate with τ_x/τ_ℓ and with the capture efficiency which is governed by the defects' density and distance from the ML. We have considered the Fröhlich interaction ($\lambda = E'_2$) and assumed that the density of localized electrons is $n_d = 4 \times 10^{11} \text{ cm}^{-2}$, and that $\tau_\ell = 10\tau_x$ following time-resolved PL experiments [39, 40]. Importantly, the intensity ratio between X^p and X^0 should not change qualitatively when one invokes advanced techniques to calculate the PL compared with the simple approach we have been using in Fig. 3(b).

Before we discuss the implications of the results, it is emphasized that optical transitions next to localization centers do not play a significant role in absorption-type experiments such as differential reflectance spectroscopy. In these measurements, one probes the oscillator strength of delocalized exciton and trion states. The signature of defects in the absorption spectrum is manifested through broadening effects. On the other hand, radiative recombination next to localized electrons is significant in the emission process because thermalized excitons can be captured before entering the minuscule light cone region.

We now turn to discussion of the results, focusing first on the distinction between radiative recombinations that involve real and virtual trions. The latter requires emission of an optical phonon during the radiative process, rendering the distinction straightforward if the energy difference between $E_X - E_\lambda$ and $E_T - E_\ell$ is noticeable. This scenario is somewhat applicable in sulfur-based MLs. For example, recombination with virtual trions in ML-WS₂ has a spectral line at $E_\lambda \sim 44 \text{ meV}$ (356 cm^{-1}) below X^0 , whereas the spectral line from real trions has a fine-structure doublet at ~ 30 and $\sim 37 \text{ meV}$ below X^0 [41]. The distinction is more subtle in ML-WSe₂ where the phonon-related spectral line nearly resonates with one of the doublet features ($\sim 30 \text{ meV}$ below X^0) [20, 24]. In this case, the gate-voltage dependence of the PL can be used to identify the recombination process. The phonon-related peak is often observed at small gate voltages whereas the trion doublet emerges at large gate voltages [24, 42, 43]. The reason is that increasing the electron density by the gate eventually screens the charged defects and electrons become delocalized. The capture process is then suppressed. In this limit, the doublet feature in the PL comes from delocalized trions.

The distinction between radiative recombinations with real and virtual trions is more subtle in MoSe₂ where the emission from trions has a single feature. However, we

can still recognize the effect of localization by comparing the absorption and emission spectra of a gated device. If the suspected peak appears in both spectra at the same voltage level, then it should be associated with delocalized trion states. On the other hand, it should be associated with localized trion states if it is absent in the absorption spectrum. Clearly, removing extrinsic defects from the substrate suppresses the recombination next to localization centers. This behavior was indeed observed by Ajayi *et al.*, who showed that **passivation** treatment of the SiO₂ substrate led to substantial suppression of the low-energy peak in the emission spectrum [44].

Other than the dependencies on sample quality and gate voltage, localization effects can be inferred from the temperature dependence of the PL. The **phonon-assisted** recombination decays with temperature because (i) excitons gain kinetic energy making them less susceptible to the capture process, as shown in Fig. 3(a), and (ii) **localized electrons that mediate the recombination process** escape the localization center. The decay of delocalized trions with temperature, on the other hand, is governed by thermal dissociation of the complex into delocalized electron and exciton. PL experiments in ML-TMDs often show that the decay already occurs when $k_B T \ll (E_X - E_{T'})$, where $E_{T'}$ is the energy of a delocalized trion. This behavior implies a dominant contribution from recombination next to localization centers, as was recently suggested by Godde *et al.* [45]. In addition, it is supported by the fact that μ -PL experiments show that the emission of the low-energy peak is localized in nature compared to the spatially homogeneous emission of neutral excitons [46, 47].

Finally, we believe that the **phonon-assisted recombination process** supports the findings of recent experiments that probed biexcitons and five-particle complexes in ML-WSe₂ [48–51]. The energy difference between the biexciton and five-particle peaks is 32 meV in all of these reports, in which the ML was encapsulated in thin hexagonal boron-nitride layers and the whole heterostructure was supported on SiO₂ substrate. The same energy difference is measured between the exciton and phonon-assisted peaks in similar devices [24]. Our claim is that the five-particle complex observed in these PL experiments is phonon-assisted recombination of biexcitons mediated by localized electrons. It starts when a localized electron virtually captures a delocalized biexciton by emitting a phonon, where the biexciton comprises dark and bright exciton components (electrons with the same spin but different valleys). Next, a photon is emitted from the intermediate virtual five-particle state. The final state is the localized electron, delocalized dark exciton, phonon and a photon. We will present a detailed study of this subject in the near future.

In conclusion, we have unravelled an intriguing phonon-assisted radiative process in the photoluminescence of monolayer transition-metal dichalcogenides. It

starts when a localized electron virtually captures the exciton by emitting a phonon, followed by photon emission from the intermediate virtual trion state. Overall, it is a strong process because $E_T - E_\ell$ nearly resonates with $E_X - E_\lambda$ where $E_{T(\ell)}$ is the energy of a localized trion (electron) and $E_{X(\lambda)}$ is the energy of an exciton (optical phonon). It is this resonance condition that led to widespread confusion, where the radiative recombination was often attributed to real trions instead of virtual ones; participation of optical phonons in the radiative process was largely ignored. We have discussed ways to distinguish between radiative recombinations with real and virtual trions based on the energy of the emitted photons. Furthermore, ways to probe localization effects were analyzed by comparing the absorption and emission spectra, as well as by using device quality, gate voltage, temperature, and magnetic field as knobs in photoluminescence experiments.

The work at the University of Rochester was mostly supported by the Department of Energy, Basic Energy Sciences, under Contract No. DE-SC0014349, whereas the computational work was also supported by the National Science Foundation (Grant No. DMR-1503601). Work at the University of Washington was supported by the Department of Energy, Basic Energy Sciences, Materials Sciences and Engineering Division (DE-SC0018171).

* hanan.dery@rochester.edu

- [1] K. Kaasbjerg, K. S. Thygesen, and K.W. Jacobsen, Phonon-limited mobility in n-type single-layer MoS₂ from first principles, *Phys. Rev. B* **85**, 115317 (2012).
- [2] T. Sohler, M. Calandra, and F. Mauri, Two-dimensional Fröhlich interaction in transition-metal dichalcogenide monolayers: Theoretical modeling and first-principles calculations, *Phys. Rev. B* **94**, 085415 (2016).
- [3] A. Thilagam, Exciton formation assisted by longitudinal optical phonons in monolayer transition metal dichalcogenides, *J. Appl. Phys.* **120**, 124306 (2016).
- [4] Y. Xiao, Z. Q. Li, and Z. W. Wang, Polaron effect on the bandgap modulation in monolayer transition metal dichalcogenides, *J. Phys. Condens. Matter.* **29**, 045001 (2017).
- [5] R. Fivaz and E. Mooser, Mobility of charge carriers in semiconducting layer structures, *Phys. Rev.* **163**, 743 (1967).
- [6] T. Cheiwchanchamnangij, W. R. L. Lambrecht, Y. Song and H. Dery, Strain effects on the spin orbit-induced band structure splittings in monolayer MoS₂ and graphene, *Phys. Rev. B* **88**, 155404 (2013).
- [7] Y. Song and H. Dery, Transport theory of monolayer transition-metal dichalcogenides through symmetry, *Phys. Rev. Lett.* **111**, 026601 (2013).
- [8] D. Y. Qiu, F. H. da Jornada, and S. G. Louie, Optical spectrum of MoS₂: many-body effects and diversity of exciton states, *Phys. Rev. Lett.* **111**, 216805 (2013).
- [9] K. Kaasbjerg, K. S. Bhargavi, S. S. Kubakaddi, Hot-electron cooling by acoustic and optical phonons in monolayers of MoS₂ and other transition-metal dichalcogenides, *Phys. Rev. B* **90**, 165436 (2014).
- [10] O. Salehzadeh, N. H. Tran, X. Liu, I. Shih, and Z. Mi, Exciton kinetics, quantum efficiency, and efficiency droop of monolayer MoS₂ light-emitting devices, *Nano. Lett.* **14**, 4125 (2014).
- [11] B. R. Carvalho, L. M. Malard, J. M. Alves, C. Fantini, and M. A. Pimenta, Symmetry-dependent exciton-phonon coupling in 2D and bulk MoS₂ observed by resonance Raman scattering, *Phys. Rev. Lett.* **114**, 136403 (2015).
- [12] G. Wang, M. M. Glazov, C. Robert, T. Amand, X. Marie, and B. Urbaszek, Double resonant Raman scattering and valley coherence generation in monolayer WSe₂, *Phys. Rev. Lett.* **115**, 117401 (2015).
- [13] G. Moody, C. K. Dass, K. Hao, C.-H. Chen, L.-J. Li, A. Singh, K. Tran, G. Clark, X. Xu, G. Berghäuser, E. Malic, A. Knorr, and X. Li, Intrinsic homogeneous linewidth and broadening mechanisms of excitons in monolayer transition metal dichalcogenides, *Nat. Commun.* **6**, 8315 (2015).
- [14] H. Dery and Y. Song, Polarization analysis of excitons in monolayer and bilayer transition-metal dichalcogenides, *Phys. Rev. B* **92**, 125431 (2015).
- [15] P. Dey, J. Paul, Z. Wang, C. E. Stevens, C. Liu, A. H. Romero, J. Shan, D. J. Hilton, and D. Karauskaj, Optical coherence in atomic-monolayer transition-metal dichalcogenides limited by electron-phonon interactions, *Phys. Rev. Lett.* **116**, 127402 (2016).
- [16] M. Danovich, I. Aleiner, N. D. Drummond, and V. Fal'ko, Fast relaxation of photo-excited carriers in 2D transition metal dichalcogenides, *IEEE J. Sel. Top. Quantum Electron.* **23**, 6000105 (2017).
- [17] C. M. Chow, H. Yu, A. M. Jones, J. R. Schaibley, M. Koehler, D. G. Mandrus, R. M., W. Yao, and X. Xu, Phonon-assisted oscillatory exciton dynamics in monolayer MoSe₂, *npj 2D Materials and Applications* **1**, 33 (2017).
- [18] D. Van Tuan, M. Yang, and H. Dery, Coulomb interaction in monolayer transition-metal dichalcogenides, *Phys. Rev. B* **98**, 125308 (2018).
- [19] S. Shree, M. Semina, C. Robert, B. Han, T. Amand, A. Balocchi, M. Manca, E. Courtade, X. Marie, T. Taniguchi, K. Watanabe, M. M. Glazov, and B. Urbaszek, Observation of exciton-phonon coupling in MoSe₂ monolayers, *Phys. Rev. B* **98**, 035302 (2018).
- [20] A. M. Jones, H. Yu, J. Schaibley, J. Yan, D. G. Mandrus, T. Taniguchi, K. Watanabe, H. Dery, W. Yao, and X. Xu, Excitonic luminescence upconversion in a two-dimensional semiconductor, *Nat. Phys.* **12**, 323 (2016).
- [21] J. Jadczyk, A. Delgado, L. Bryja, Y. S. Huang, and P. Hawrylak, Robust high-temperature trion emission in monolayers of Mo(S_ySe_{1-y})₂ alloys, *Phys. Rev. B* **95**, 195427 (2017).
- [22] A. M. Jones, H. Yu, N. J. Ghimire, S. Wu, G. Aivazian, J. S. Ross, B. Zhao, J. Yan, D. G. Mandrus, D. Xiao, W. Yao, and X. Xu, Optical generation of excitonic valley coherence in monolayer WSe₂, *Nat. Nano.* **8**, 634 (2013).
- [23] Z. Wang, L. Zhao, K. F. Mak, and J. Shan, Probing the spin-polarized electronic band structure in monolayer transition metal dichalcogenides by optical spectroscopy, *Nano Lett.* **17**, 740 (2017).
- [24] E. Courtade, M. Semina, M. Manca, M. M. Glazov, C. Robert, F. Cadiz, G. Wang, T. Taniguchi, K. Watanabe,

- M. Pierre, W. Escoffier, E. L. Ivchenko, P. Renucci, X. Marie, T. Amand, and B. Urbaszek, Charged excitons in monolayer WSe₂: experiment and theory, *Phys. Rev. B* **96**, 085302 (2017).
- [25] D. Van Tuan, B. Scharf, I. Žutić, and H. Dery, Marrying excitons and plasmons in monolayer transition-metal dichalcogenides, *Phys. Rev. X* **7**, 041040 (2017).
- [26] H. Fröhlich, Electrons in lattice fields, *Advances in Physics* **3**, 325 (1954).
- [27] R. P. Feynman, Slow electrons in a polar crystal, *Phys. Rev.* **97**, 660 (1955).
- [28] P. Y. Yu and M. Cardona, *Fundamentals of Semiconductors*, 3rd ed. (Springer, Berlin, 2005).
- [29] A. J. Shields, C. Trallero-Giner, M. Cardona, H. T. Grahn, K. Ploog, V. A. Haisler, D. A. Tenne, N. T. Moshegov, and A. I. Toropov, Resonant Raman scattering in GaAs/AlAs superlattices under electric fields, *Phys. Rev. B* **46**, 6990 (1992).
- [30] K. Huang and R. Rhys, Theory of light absorption and non-radiative transitions in F-centres, *Proc. R. Soc.* **204**, 406 (1950).
- [31] K. Varga and Y. Suzuki, Precise solution of few-body problems with the stochastic variational method on a correlated Gaussian basis, *Phys. Rev. C* **52**, 2885 (1995).
- [32] K. Varga, Solution of few-body problems with the stochastic variational method II: Two-dimensional systems, *Comp. Phys. Comm.* **179**, 591 (2008).
- [33] J. Mitroy, S. Bubin, W. Horiuchi, Y. Suzuki, L. Adamowicz, W. Cencek, K. Szalewicz, J. Komasa, D. Blume, and K. Varga, Theory and application of explicitly correlated Gaussians, *Rev. Mod. Phys.* **85**, 693 (2013).
- [34] D. W. Kidd, D. K. Zhang, and K. Varga, Binding energies and structures of two-dimensional excitonic complexes in transition metal dichalcogenides, *Phys. Rev. B* **93**, 125423 (2016).
- [35] M. Van der Donck, M. Zarenia, and F. M. Peeters, Excitons and trions in monolayer transition metal dichalcogenides: A comparative study between the multiband model and the quadratic single-band model, *Phys. Rev. B* **96**, 035131 (2017).
- [36] See Supplemental Material for details on the Coulomb potentials in Eq. (1), analysis of the various electron-phonon interactions in Eq. (2), the derivation of Eq. (3), the dependencies of the phonon-assisted recombination on magnetic field, temperature, and distance of the impurity from the substrate, and a compiled list of parameter values used in the simulations. It includes Refs. [52]-[59].
- [37] I. Žutić, A. Matos-Abiague, B. Scharf, H. Dery, and K. Belashchenko, Proximitized materials, *Mater. Today* (2018), doi: 10.1016/j.mattod.2018.05.003.
- [38] Haining Wang, Changjian Zhang, Weimin Chan, Christina Manolatu, Sandip Tiwari, and Farhan Rana, Radiative lifetimes of excitons and trions in monolayers of the metal dichalcogenide MoS₂, *Phys. Rev. B* **93**, 045407 (2016).
- [39] C. Robert, D. Lagarde, F. Cadiz, G. Wang, B. Lassagne, T. Amand, A. Balocchi, P. Renucci, S. Tongay, B. Urbaszek, and X. Marie, Exciton radiative lifetime in transition metal dichalcogenide monolayers, *Phys. Rev. B* **93**, 205423 (2016).
- [40] G. Wang, L. Bouet, D. Lagarde, M. Vidal, A. Balocchi, T. Amand, X. Marie, and B. Urbaszek, Valley dynamics probed through charged and neutral exciton emission in monolayer WSe₂, *Phys. Rev. B* **90**, 075413 (2014).
- [41] G. Plechinger, P. Nagler, A. Arora, R. Schmidt, A. Chernikov, A. Granados del Águila, P. C. M. Christianen, R. Bratschitsch, C. Schüller, and T. Korn, Trion Fine Structure and Coupled Spin-Valley Dynamics in Monolayer Tungsten Disulfide, *Nat. Commun.* **7**, 12715 (2016).
- [42] Y. Zhou, G. Scuri, D. S. Wild, A. A. High, A. Dibos, L. A. Jauregui, C. Shu, K. De Greve, K. Pistunova, A. Y. Joe, T. Taniguchi, K. Watanabe, P. Kim, M. D. Lukin, and H. Park, Probing dark excitons in atomically thin semiconductors via near-field coupling to surface plasmon polaritons, *Nat. Nanotechnol.* **12**, 856 (2017).
- [43] G. Wang, A. Chernikov, M. M. Glazov, T. F. Heinz, X. Marie, T. Amand, and B. Urbaszek, Colloquium: Excitons in atomically thin transition metal dichalcogenides, *Rev. Mod. Phys.* **90**, 021001 (2018).
- [44] O. A. Ajayi, J. V. Ardelean, G. D. Shepard, J. Wang, A. Antony, T. Taniguchi, K. Watanabe, T. F. Heinz, S. Strauf, and X.-Y. Zhu, Approaching the intrinsic photoluminescence linewidth in transition metal dichalcogenide monolayers, *2D Mater.* **4**, 031011 (2017).
- [45] T. Godde, D. Schmidt, J. Schmutzler, M. Amann, J. Debus, F. Withers, E. M. Alexeev, O. Del Pozo-Zamudio, O. V. Skrypka, K. S. Novoselov, M. Bayer, and A. I. Tartakovskii, Exciton and trion dynamics in atomically thin MoSe₂ and WSe₂: Effect of localization, *Phys. Rev. B* **94**, 165301 (2016).
- [46] W. Bao, N. J. Borys, C. Ko, J. Suh, W. Fan, A. Thron, Y. Zhang, A. Buyanin, J. Zhang, S. Cabrini, P. D. Ashby, A. Weber-Bargioni, S. Tongay, S. Aloni, D. F. Ogletree, J. Wu, M. B. Salmeron, and P. J. Schuck, Visualizing nanoscale excitonic relaxation properties of disordered edges and grain boundaries in monolayer molybdenum disulfide, *Nat. Commun.* **6**, 7993 (2015).
- [47] A. Neumann, J. Lindlau, M. Nutz, A. D. Mohite, H. Yamaguchi, and A. Högele, Signatures of defect-localized charged excitons in the photoluminescence of monolayer molybdenum disulfide, *Phys. Rev. Mater.* **2**, 124003 (2018).
- [48] S.-Y. Chen, T. Goldstein, T. Taniguchi, K. Watanabe, and J. Yan, Coulomb-bound four- and five-particle intervalley states in an atomically-thin semiconductor, *Nat. Commun.* **9**, 3717 (2018).
- [49] Z. Ye, L. Waldecker, E. Y. Ma, D. Rhodes, A. Antony, B. Kim, X.-X. Zhang, M. Deng, Y. Jiang, Z. Lu, D. Smirnov, K. Watanabe, T. Taniguchi, J. Hone, and T. F. Heinz, Efficient generation of neutral and charged biexcitons in encapsulated WSe₂ monolayers, *Nat. Commun.* **9**, 3718 (2018).
- [50] Z. Li, T. Wang, Z. Lu, C. Jin, Y. Chen, Y. Meng, Z. Lian, T. Taniguchi, K. Watanabe, S. Zhang, D. Smirnov, and S.-F. Shi, Revealing the biexciton and trion-exciton complexes in BN encapsulated WSe₂, *Nat. Commun.* **9**, 3719 (2018).
- [51] M. Barbone, A. R.-P. Montblanch, D. M. Kara, C. Palacios-Berraquero, A. R. Cadore, D. De Fazio, B. Pingault, E. Mostaani, H. Li, B. Chen, K. Watanabe, T. Taniguchi, S. Tongay, G. Wang, A. C. Ferrari, and M. Atatüre, Charge-tuneable biexciton complexes in monolayer WSe₂, *Nat. Commun.* **9**, 3721 (2018).
- [52] P. Cudazzo, I. V. Tokatly, and A. Rubio, Dielectric screening in two-dimensional insulators: Implications for excitonic and impurity states in graphane, *Phys. Rev. B* **84**, 085406 (2011).

- [53] E. Mostaani, M. Sznyszewski, C. H. Price, R. Maezono, M. Danovich, R. J. Hunt, N. D. Drummond, and V. I. Fal'ko, Diffusion quantum Monte Carlo study of excitonic complexes in two-dimensional transition-metal dichalcogenides, *Phys. Rev. B* **96**, 075431 (2017).
- [54] W. M. C. Foulkes, L. Mitas, R. J. Needs, and G. Rajagopal, Quantum Monte Carlo simulations of solids, *Rev. Mod. Phys.* **73**, 33 (2001).
- [55] S. Permogorov , Optical emission due to exciton scattering by LO phonons in semiconductors, in *Excitons*, edited by E. I. Rashba and M. D. Sturge (North Holland, Amsterdam, 1979), pp. 177-204.
- [56] W. Kohn and J. M. Luttinger, Hyperfine Splitting of Donor States in Silicon, *Phys. Rev.* **97**, 883 (1955).
- [57] W. Kohn, Shallow impurity states in silicon and germanium, in *Solid State Physics*, edited by F. Seitz and D. Turnbull (Academic Press, New York, 1957), Vol. 5, pp. 257-320.
- [58] G. Plechinger, P. Nagler, A. Arora, A. Granados del Águila, M. V. Ballottin, T. Frank, P. Steinleitner, M. Gmitra, J. Fabian, P. C. M. Christianen, R. Bratschitsch, C. Schüller, and T. Korn, Excitonic Valley Effects in Monolayer WS₂ under High Magnetic Fields, *Nano Lett.* **16**, 7899 (2016).
- [59] A. Kormányos, G. Burkard, M. Gmitra, J. Fabian, V. Zólyomi, N. D. Drummond, and V. Fal'ko, $\mathbf{k} \cdot \mathbf{p}$ theory for two-dimensional transition metal dichalcogenide semiconductors, *2D Mater.* **2**, 022001 (2015).